OPTICS

# Ultra-broadband all-optical sampling of optical waveforms

**Dmitry A. Zimin[1,2], Vladislav S. Yakovlev[1,2], Nicholas Karpowicz[1,3]***

**Optical-field sampling techniques provide direct access to the electric field of visible and near-infrared light. The existing methods achieve the necessary bandwidth using highly nonlinear light-matter interaction that involves ionization of atoms or generation of charge carriers in solids. We demonstrate an alternative, all-optical approach for measuring electric fields of broadband laser pulses, which offers an advantage in terms of sensitivity and signal-to-noise ratio and extends the detection bandwidth of optical methods to the petahertz domain.**



## INTRODUCTION

Direct access to the electric field of light (*1*) provides a subcycle view of the polarization response of matter (*2*), thus enabling sensitive metrology in physics (*3*–*7*), chemistry (*8*), and medicine (*9*, *10*). Optical-field sampling techniques take advantage of some process that lasts much less than an optical cycle of the measured light wave. Most of them rely on the generation of free electrons either by a weak extreme ultraviolet pulse (*11*–*13*) or by a strong optical pulse (*14*–*23*). An alternative is all-optical methods, where the fast process is a nonlinear wave mixing. Such photonic methods may rely on extreme ultraviolet (*24*–*26*) or optical pulses (*27*–*30*). They typically have a better sensitivity (*10*, *27*, *31*) but a smaller cutoff frequency. Here, we propose generalized heterodyne optical-sampling techniques (GHOSTs), which overcome the bandwidth limit through controlling light-pulse waveforms. Combinations of multiple nonlinear optical processes allow new detection bands to be placed throughout the electromagnetic spectrum, enabling all-optical waveform sampling in the visible and ultraviolet spectral ranges.

Let us review the fundamental form of nonlinear optics–based field-sampling techniques that exist for the infrared and terahertz domains (see Fig. 1). In these techniques, the field that is being sampled (test field) undergoes nonlinear wave mixing with a sampling pulse that creates a temporal gate. The outcome of this nonlinear interaction is referred to as heterodyne signal or, for brevity, simply signal, although this is not yet the outcome of the measurement. This signal is first made to interfere with the local oscillator (LO), which is what the sampling pulse becomes after transmission through the same nonlinear medium in the absence of the test field. In a spectral region where the signal and the LO overlap, the spectral intensity of their superposition depends on the delay between the test and sampling pulses. Two prominent examples of such measurement techniques are electro-optic sampling (EOS) (*27*–*30*) and air-biased coherent detection (ABCD) (*31*, *32*). In EOS, the signal is produced from sum and difference frequency generation between the test waveform and sampling pulse, and the LO is provided by the unperturbed sampling pulse (*30*, 33). In ABCD, the signal is the result of four-wave mixing, summing two photons from the sampling pulse and subtracting one from the test waveform, while the LO is provided by field-induced second harmonic generation: A bias applied to the nonlinear medium allows it to combine two sampling-pulse photons even if the medium is centrosymmetric. The phase of the nonlinearly created LO is modulated by changing the direction of the bias field. This modulation creates sidebands of the LO, which interfere with the signal, thus enabling heterodyne detection of pulses over a continuous range from the terahertz through the mid-infrared (*31*).

In addition to the spectral overlap between the signal and the LO, these schemes had to satisfy two key requirements: (i) Only one photon from the test waveform is involved in the generation of the signal, and (ii) the same number of photons from the sampling pulse is involved in forming the LO and signal. The former is necessary for linear detection of the field. The latter ensures that the interference between the signal and the LO is insensitive to the carrier-envelope phase (CEP) of the sampling pulse, which is known as the global phase (*29*) for arbitrary waveforms. If requirement (ii) is satisfied, the phase cancels during heterodyne detection, meaning that sampling pulses with unstable CEP can be used. When both these requirements are fulfilled, the interference between the signal and LO has an amplitude and phase determined by the test waveform, and varying the delay between the pulses while recording the resulting intensity measures the electric field of the test waveform.

Requirement (ii) is responsible for the primary limit on the maximum detection frequency of the techniques: Since the signal and LO wavelengths must match, and the signal frequency is shifted by the frequency of the test waveform, it cannot exceed the bandwidth of the LO. However, the emergence of CEP-stabilized mode-locked laser oscillators allows us to bypass this restriction. For example, using second harmonic generation to form the LO for a signal based on sum-frequency generation (SFG), i.e., adding one more photon from the sampling pulse to the LO of EOS, increases the frequency of the detection band by the carrier frequency of the sampling pulse. We label this GHOST as SFG + second harmonic generation (SHG). A 5-fs sampling pulse at 400-THz carrier frequency and 200-THz bandwidth, capable of detecting 0 to 200 THz via EOS, could in principle detect 100 to 700 THz via SFG + SHG (Fig. 1) or 900 to 1500 THz via difference-frequency generation (DFG) + SHG. Other GHOSTs, on the other hand, may in principle be used to detect even higher spectral components. Using CEP-stable pulses, the detection bandwidth and

[1]Max-Planck-Institut für Quantenoptik, Hans-Kopfermann-Strasse 1, 85748, Garching, Germany. [2]Fakultät für Physik, Ludwig-Maximilians-Universität, Am Coulombwall 1, 85748, Garching, Germany. [3]CNR NANOTEC Institute of Nanotechnology, via Monteroni, Lecce 73100, Italy.
*Corresponding author. Email: nicholas.karpowicz@mpq.mpg.de

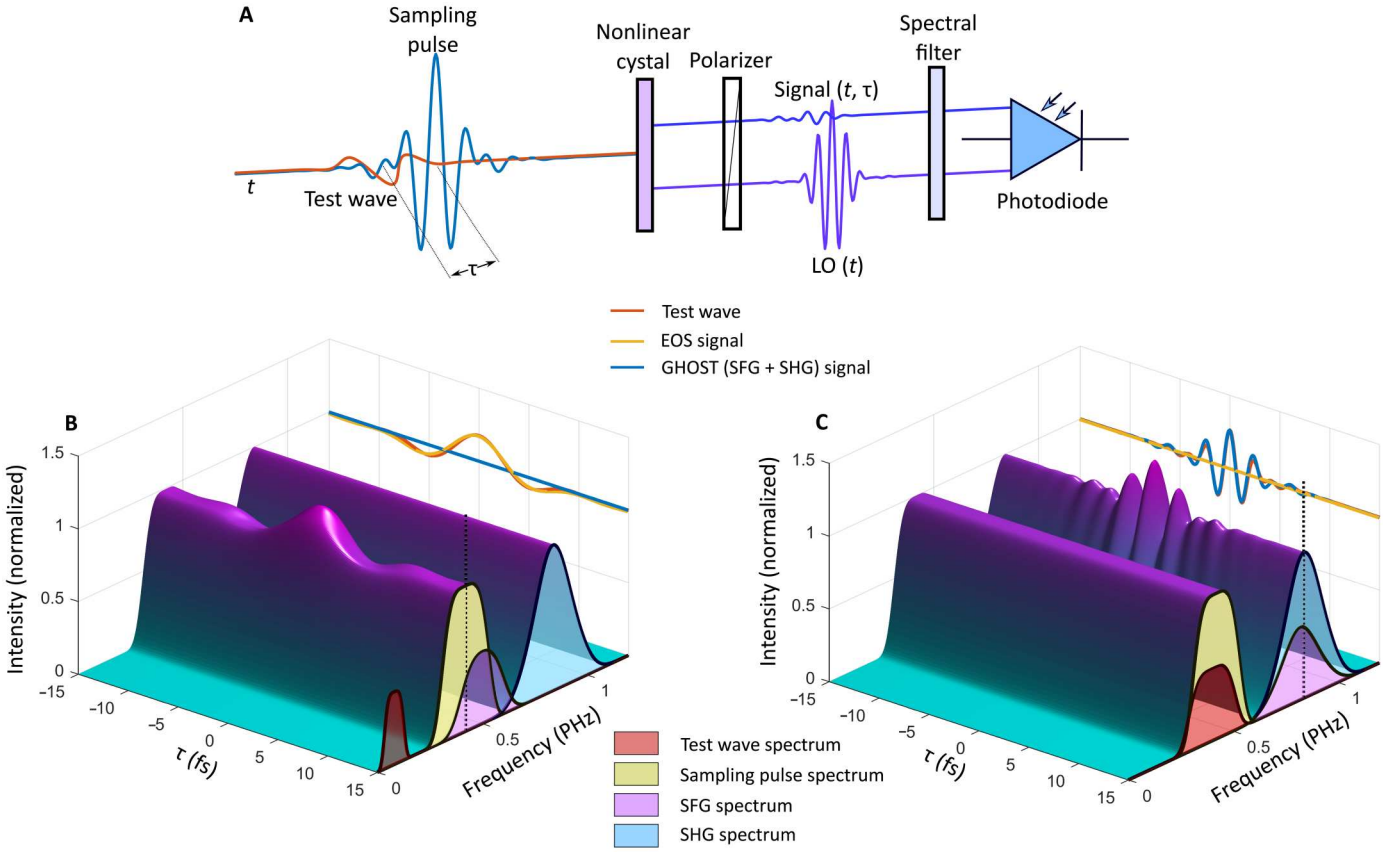


**Fig. 1. Illustration of the measurement concept.** (**A**) Two pulses are incident on the nonlinear medium: a test waveform that we wish to measure and a sampling pulse that will be used to probe its structure. Two waves emerge from the crystal: an LO, which is formed by nonlinear propagation of the sampling pulse, and a signal, which is the product of nonlinearly mixing both input pulses. These pass through a polarizer and a band-pass spectral filter, and the intensity of the light is recorded in a photodiode. (**B**) In the case of EOS, sum-frequency generation (SFG) forms the signal that primarily overlaps with the unmodified spectrum of the sampling pulse. The interference of the signal with the LO modulates the spectral intensity versus time delay τ. At the detection frequency, labeled with a vertical dashed line, the amplitude traces out the electric field waveform, providing the EOS signal. (**C**) For a test pulse in the visible spectral range, the SFG spectrum lies at higher frequencies, predominantly in the ultraviolet, and has little spectral overlap with the sampling pulse. However, it significantly overlaps with the second harmonic of the sampling pulse that was generated in the same nonlinear crystal, permitting the SFG + SHG GHOST to take place. The modulation of spectral intensity in the ultraviolet band, at the detection frequency marked by the dashed line, traces out the test waveform. This concept can be extended to detection of light in other spectral regions, requiring a combination of nonlinear processes to produce spectrally overlapping signal and LO waves.

spectral ranges can be expanded and tailored by choosing appropriate combinations of GHOSTs and detection frequencies (see the Supplementary Materials). The price that one pays for this is that the phases of the LO and signal experience a different phase shift upon a change of the CEP of the sampling pulse. As a result, a phase shift $\Delta\phi_{CE} = a\,(N_S - N_{LO})\,\phi_S$ is applied to the measured waveform, where $N_S$ is the number of sampling-pulse photons summed over to arrive at the signal, $N_{LO}$ is the number of photons that participate in generating a photon of the LO, $a$ is 1 or −1 depending on the mixing process, and $\phi_S$ is the CEP of the sampling pulse (for further details, see the Supplementary Materials).

In both EOS and ABCD, $\Delta\phi_{CE} = 0$, while in the SFG + SHG GHOST, $\Delta\phi_{CE} = -\phi_S$. This has a straightforward interpretation in the time domain: In any linear electric-field measurement, the detected waveform is the convolution of the true electric field with the response function of the detection system. The addition of an unbalanced photon in the detection scheme causes this response function to oscillate in time, which allows for the detection of more rapidly varying fields, but repeated measurements of fields with reproducible (CEP-stabilized) waveforms will average to zero if $\phi_S$ is not stabilized.

The sampling pulse must be well characterized for this response function to be determined, which is necessary to relate the measured waveform back to the original electric field. If the sampling pulse is not compressed, the amplitude of the response will be weak due to destructive interference between contributions from different spectral components of the pulse.

## RESULTS

To confirm the validity of the concept, we experimentally investigated the "SFG/DFG + THG" GHOST using a 2.7-fs pulse (*18*), whose spectrum is presented in Fig. 2 (shaded magenta curve), where SFG and DFG together form the heterodyne signal, while third-harmonic generation (THG) forms the LO (see the Supplementary Materials for further details). As a nonlinear medium

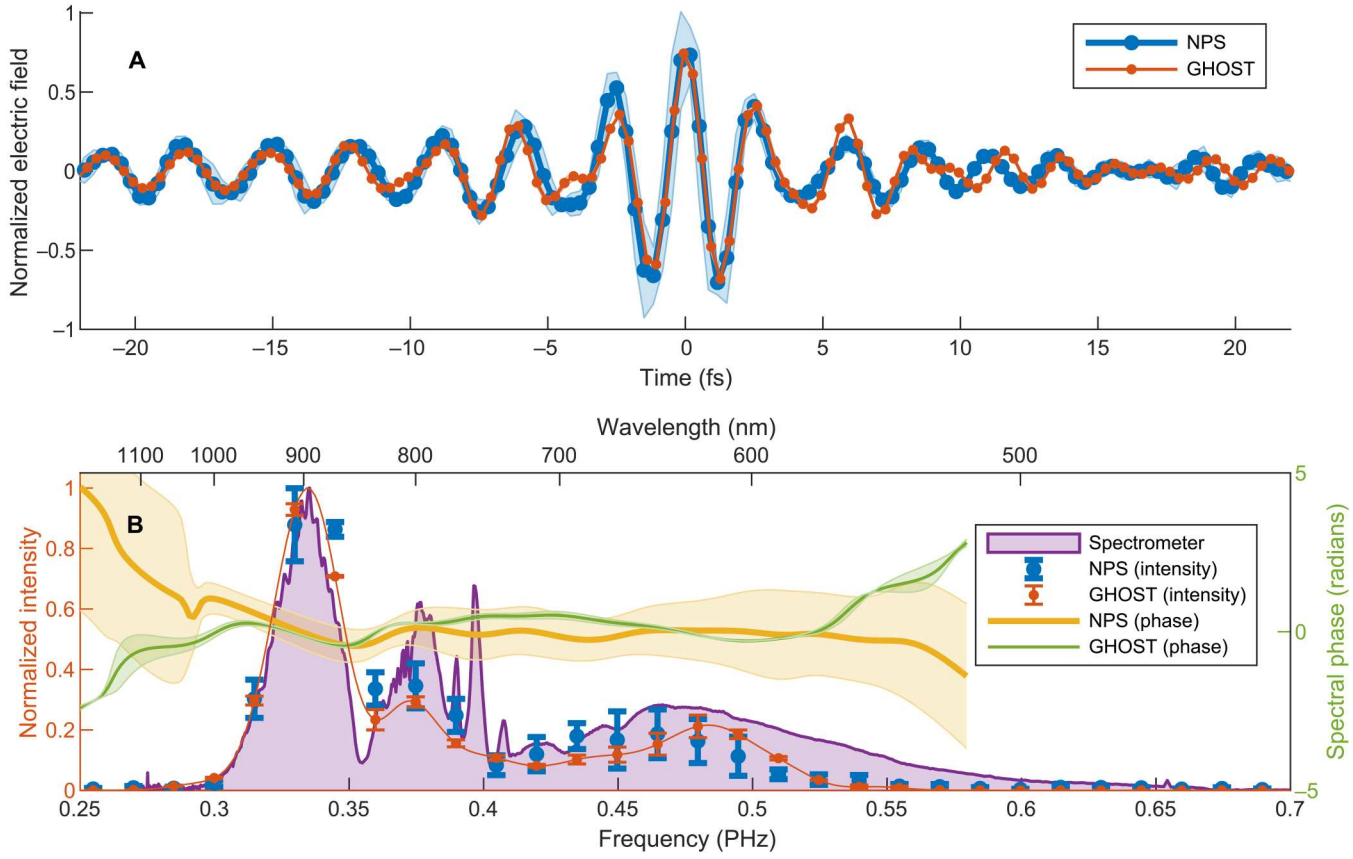


**Fig. 2. Validation of GHOST detection via benchmarking against NPS and spectrometry.** (**A**) Electric-field waveforms measured with the SFG/DFG + THG GHOST and NPS. Using SFG signals, this GHOST allows for detection in the visible and ultraviolet, from approximately 0.1 to 0.7 PHz (see the Supplementary Materials for details). The shaded areas represent the SDs evaluated from three individual measurements. (**B**) The spectral intensities and phases of the waveforms shown in (A) and the spectrum obtained by a grating spectrometer. The shaded areas show the SDs for the spectral phases. We depicted SDs of the spectral intensities with error bars.

that has both $\chi^{(2)}$ and $\chi^{(3)}$ nonlinearities, we chose a thin quartz crystal (see the Supplementary Materials for details) for its low absorption and dispersion. For detection, we used a band-pass filter that transmitted light between 0.83 and 0.86 PHz (see the Supplementary Materials). Although this frequency range is in the middle of the second harmonic of the sampling pulse, the orientations of the crystal and the polarizer were chosen such that only the $\chi^{(3)}$ nonlinearity contributed to the LO. We benchmarked this implementation of GHOST against nonlinear photoconductive sampling (NPS) (*18*), which is a field-sampling technique where temporal gating is achieved through highly nonlinear photoinjection of charge carriers. Both GHOST and NPS measurements were performed using a 2.7-fs sampling pulse, and we used theoretical response functions to retrieve time-dependent electric field from the raw measured data (see the Supplementary Materials for details). The benchmarking results are shown in Fig. 2. In the time domain (Fig. 2A), the two waveforms have very similar shapes: The Pearson correlation coefficient between the waveforms is $\rho = 0.93$. The discrepancy between the spectrum obtained with a spectrometer and with a Fourier transformation of recorded pulse waveforms is attributed to differences in the temporal and spatial gating of the two measurements. As the waveforms are measured over a finite range of time delay, spectral components outside of this time window are not included in the measurement. The spot size of the gate determines the measured spatial volume, which can also influence the measured spectrum in the presence of spatiotemporal distortions. Note that GHOST measurements show much smaller stochastic fluctuations —the peak SD is 10 times smaller than that of the NPS measurements. The spectra of both electric-field waveforms agree well with the spectrum obtained with a calibrated grating spectrometer (Ocean Optics).

The benchmarking results shown in Fig. 2 confirm only the validity of the SFG + THG GHOST; to validate the DFG + THG GHOST, the spectrum of the test pulse must extend well above the frequencies that reach the photodiode. As a simple estimation, let us take 0.3 PHz as the lowest frequency present in the sampling pulse and 0.8 PHz as the detection frequency. In this case, we expect the spectral range covered by the DFG + THG GHOST to begin at 1.1 PHz. So, we upconverted the test pulse in a 100-μm β-barium borate (BBO) crystal, obtaining pulses with a spectrum that extended up to 1.25 PHz (see the Supplementary Materials). We plot the GHOST waveform in Fig. 3A (here, no attempt is made to account for the theoretical response function). In Fig. 3B, we compare the spectrum of the detected waveform with the spectrum that we measured with a grating spectrometer. The inset displays the spectral range that is relevant to the DFG + THG GHOST. While there are discrepancies between the two spectra, and a careful benchmarking in this spectral range is yet to be done, we conclude that

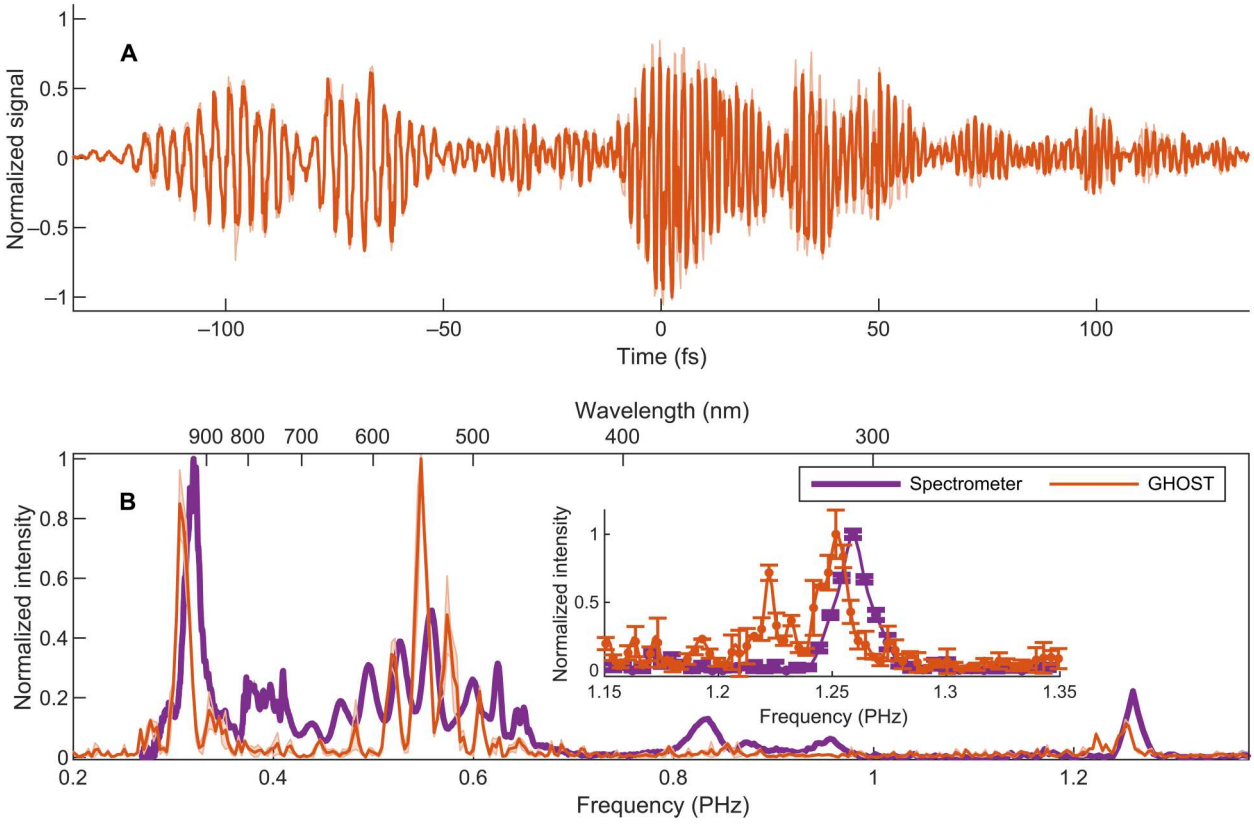


**Fig. 3. Ultraviolet waveform detection with the DFG + THG GHOST.** We demonstrate the potential bandwidth of GHOST by applying it to a test waveform generated by up-converting the pulse shown in Fig. 2. The shaded areas and error bars represent SDs. The DFG + THG GHOST has a theoretical detection window from approximately 0.9 to 1.5 PHz, although phase-matching constraints limit the signal at shorter wavelengths (see the Supplementary Materials for details). (**A**) The detected waveform contains a rapid ultraviolet oscillation preceded by the lower-frequency light (detected through the SFG + THG GHOST). The delay between the two parts of the test pulse is caused by the group velocity mismatch in the 100-μm BBO crystal that we used for up-conversion. (**B**) The spectrum of the GHOST waveform (red) and the spectrum measured by a grating spectrometer (purple).

our implementation of GHOST is capable of optical-field sampling at frequencies that exceed 1.2 PHz.

As an additional verification that we indeed implemented the SFG/DFG + THG GHOST, we investigated how the measured waveforms depend on the peak strengths of the incident sampling and test pulses. The results are shown in Fig. 4. As expected, the amplitudes of measured waveforms scale as the fourth power of the peak sampling field, $E_s$. Each photon in the heterodyne signal emerges with the involvement of one photon from the sampling pulse, while each photon in the LO emerges from a three-photon nonlinear process. Thus, the electric field of the heterodyne signal scales linearly with $E_S$, the electric field of the LO scales as $E_S^3$, and the interference between the two fields makes the intensity oscillate with an amplitude that is proportional to $E_S^4$. We observe this dependence up to sampling fields as strong as 1.5 V/Å (see Fig. 4A). At this field strength, multiphoton photoinjection of charge carriers becomes significant. According to Fig. 4B, the amplitude of the measured waveforms scales linearly up to test fields as strong as 0.5 V/Å. Nevertheless, Fig. 4C shows that already the 0.27-V/Å test pulse produces a waveform that has high-frequency components that are absent in the waveform measured with the 0.12-V/Å test pulse. From Fig. 4C, we can also estimate a typical signal-to-noise ratio (SNR) of our measurements. By comparing the noise baseline with the peak signal strength, we obtain an intensity SNR of approximately 30 dB independently of the test-field strength, which indicates that, in these measurements, the noise was dominated by the fluctuations of laser intensity. Future improvements (e.g., using a balanced detection scheme) may further improve the SNR.

## DISCUSSION

GHOSTs present a promising approach for measuring electric fields of broadband laser pulses. We studied one particular combination of nonlinear optical processes: SFG/DFG + THG, where the $\chi^{(2)}$ nonlinearity mixed the sampling and test waves, thus generating a heterodyne signal, while the third harmonic of the sampling pulse provided an LO. The spectral response of GHOST can be tailored for a particular application through the choice of nonlinear processes and the frequency range that reaches the photodetector. In principle, bandwidths exceeding 1 PHz may be achievable with a combination of different GHOSTs, with an octave-spanning sampling pulse. Any medium that exhibits the required nonlinearities, such as solids or gases, could be used for waveform sampling. Since they rely on low-order nonlinearities, GHOSTs can be used with a broad variety of laser systems that produce pulses with a stabilized

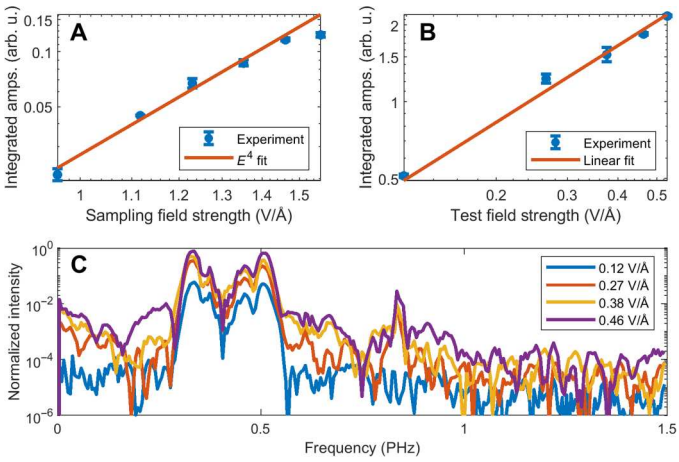


**Fig. 4. Intensity scaling and SNR.** (**A**) Scaling of the measured signal versus field strength of the sampling pulse. (**B**) Scaling the measured signal versus field strength of a test pulse. (**C**) Logarithmically scaled typical measured spectrum and spectral noise floor.

CEP. The use of low-order nonlinear processes implies that similar field-resolved detection using femtosecond oscillators is possible.

Direct time-domain measurements of light-matter interaction with subcycle resolution are at the forefront of attosecond science. The new technique for direct electric field measurement presents opportunities for highly sensitive time-resolved spectroscopy and for the extension of field-resolved metrology to regimes of both wavelength and intensity. The flexibility offered in terms of signal photon energy, detection bandwidth, and nonlinear optical processes provides an opportunity for field measurements to be integrated into a variety of new investigations.

## MATERIALS AND METHODS

The laser system used for the experiments (more details in the Supplementary Materials) comprises a Ti:sapphire oscillator (Rainbow 2, Spectra Physics), followed by chirped pulse amplification to 1-mJ pulse energy at 3-kHz repetition rate, further spectral broadening in a hollow-core fiber and a chirped mirror compressor. The experimental data acquisition (more details in the Supplementary Materials) was performed with a dual-phase lock-in amplifier (SR-830, Stanford Research Systems) and with a grating spectrometer (Ocean Optics).

## Supplementary Materials

**This PDF file includes:**

Supplementary Text
Figs. S1 to S11
Table S1
References

## REFERENCES AND NOTES


1. R. Kienberger, E. Goulielmakis, M. Uiberacker, A. Baltuska, V. Yakovlev, F. Bammer, A. Scrinzi, T. Westerwalbesloh, U. Kleineberg, U. Heinzmann, M. Drescher, F. Krausz, Atomic transient recorder. *Nature* **427**, 817–821 (2004).
2. A. Sommer, E. M. Bothschafter, S. A. Sato, C. Jakubeit, T. Latka, O. Razskazovskaya, H. Fattahi, M. Jobst, W. Schweinberger, V. Shirvanyan, V. S. Yakovlev, R. Kienberger, K. Yabana, N. Karpowicz, M. Schultze, F. Krausz, Attosecond nonlinear polarization and light–Matter energy transfer in solids. *Nature* **534**, 86–90 (2016).
3. M. Hohenleutner, F. Langer, O. Schubert, M. Knorr, U. Huttner, S. W. Koch, M. Kira, R. Huber, Real-time observation of interfering crystal electrons in high-harmonic generation. *Nature* **523**, 572–575 (2015).
4. W. Kuehn, P. Gaal, K. Reimann, M. Woerner, T. Elsaesser, R. Hey, Coherent ballistic motion of electrons in a periodic potential. *Phys. Rev. Lett.* **104**, 146602 (2010).
5. P. Gaal, W. Kuehn, K. Reimann, M. Woerner, T. Elsaesser, R. Hey, Internal motions of a quasiparticle governing its ultrafast nonlinear response. *Nature* **450**, 1210–1213 (2007).
6. R. Ulbricht, E. Hendry, J. Shan, T. F. Heinz, M. Bonn, Carrier dynamics in semiconductors studied with time-resolved terahertz spectroscopy. *Rev. Mod. Phys.* **83**, 543–586 (2011).
7. F. Schlaepfer, M. Lucchini, S. A. Sato, M. Volkov, L. Kasmi, N. Hartmann, A. Rubio, L. Gallmann, U. Keller, Attosecond optical-field-enhanced carrier injection into the gaas conduction band. *Nat. Phys.* **14**, 560–564 (2018).
8. M. Kowalewski, K. Bennett, J. R. Rouxel, S. Mukamel, Monitoring nonadiabatic electron-nuclear dynamics in molecules by attosecond streaking of photoelectrons. *Phys. Rev. Lett.* **117**, 043201 (2016).
9. M. Huber, K. V. Kepesidis, L. Voronina, M. Božić, M. Trubetskov, N. Harbeck, F. Krausz, M. Žigman, Stability of person-specific blood-based infrared molecular fingerprints opens up prospects for health monitoring. *Nat. Commun.* **12**, 1511 (2021).
10. I. Pupeza, M. Huber, M. Trubetskov, W. Schweinberger, S. A. Hussain, C. Hofer, K. Fritsch, M. Poetzlberger, L. Vamos, E. Fill, T. Amotchkina, K. V. Kepesidis, A. Apolonski, N. Karpowicz, V. Pervak, O. Pronin, F. Fleischmann, A. Azzeer, M. Žigman, F. Krausz, Field-resolved infrared spectroscopy of biological systems. *Nature* **577**, 52–59 (2020).
11. M. Hentschel, R. Kienberger, C. Spielmann, G. A. Reider, N. Milosevic, T. Brabec, P. Corkum, U. Heinzmann, M. Drescher, F. Krausz, Attosecond metrology. *Nature* **414**, 509–513 (2001).
12. J. Itatani, F. Quéré, G. L. Yudin, M. Y. Ivanov, F. Krausz, P. B. Corkum, Attosecond streak camera. *Phys. Rev. Lett.* **88**, 173903 (2002).
13. E. Goulielmakis, M. Uiberacker, R. Kienberger, A. Baltuska, V. Yakovlev, A. Scrinzi, T. Westerwalbesloh, U. Kleineberg, U. Heinzmann, M. Drescher, F. Krausz, Direct measurement of light waves. *Science* **305**, 1267–1269 (2004).
14. S. Thunich, C. Ruppert, A. W. Holleitner, M. Betz, Field-resolved characterization of femtosecond electromagnetic pulses with 400 thz bandwidth. *Opt. Lett.* **36**, 1791–1793 (2011).
15. A. Schiffrin, T. Paasch-Colberg, N. Karpowicz, V. Apalkov, D. Gerster, S. Mühlbrandt, M. Korbman, J. Reichert, M. Schultze, S. Holzner, J. V. Barth, R. Kienberger, R. Ernstorfer, V. S. Yakovlev, M. I. Stockman, F. Krausz, Optical-field-induced current in dielectrics. *Nature* **493**, 70–74 (2013).
16. S. B. Park, K. Kim, W. Cho, S. I. Hwang, I. Ivanov, C. H. Nam, K. T. Kim, Direct sampling of a light wave in air. *Optica* **5**, 402–408 (2018).
17. M. Kubullek, Z. Wang, K. von der Brelje, D. Zimin, P. Rosenberger, J. Schötz, M. Neuhaus, S. Sederberg, A. Staudte, N. Karpowicz, M. F. Kling, B. Bergues, Single-shot carrier–Envelope-phase measurement in ambient air. *Optica* **7**, 35 (2020).
18. S. Sederberg, D. Zimin, S. Keiber, F. Siegrist, M. S. Wismer, V. S. Yakovlev, I. Floss, C. Lemell, J. Burgdörfer, M. Schultze, F. Krausz, N. Karpowicz, Attosecond optoelectronic field measurement in solids. *Nat. Commun.* **11**, 430 (2020).
19. D. Zimin, M. Weidman, J. Schötz, M. F. Kling, V. S. Yakovlev, F. Krausz, N. Karpowicz, Petahertz-scale nonlinear photoconductive sampling in air. *Optica* **8**, 586–590 (2021).
20. W. Cho, S. I. Hwang, C. H. Nam, M. R. Bionta, P. Lassonde, B. E. Schmidt, H. Ibrahim, F. Légaré, K. T. Kim, Temporal characterization of femtosecond laser pulses using tunneling ionization in the UV, visible, and mid-IR ranges. *Sci. Rep.* **9**, 16067 (2019).
21. J. Blöchl, J. Schötz, A. Maliakkal, N. Šreibere, Z. Wang, P. Rosenberger, P. Hommelhoff, A. Staudte, P. B. Corkum, B. Bergues, M. F. Kling, Spatiotemporal sampling of near-petahertz vortex fields. *Optica* **9**, 755–761 (2022).
22. Y. Liu, J. E. Beetar, J. Nesper, S. Gholam-Mirzaei, M. Chini, Single-shot measurement of few-cycle optical waveforms on a chip. *Nat. Photonics* **16**, 109–112 (2022).
23. M. R. Bionta, F. Ritzkowsky, M. Turchetti, Y. Yang, D. C. Mor, W. P. Putnam, F. X. Kärtner, K. K. Berggren, P. D. Keathley, On-chip sampling of optical fields with attosecond resolution. *Nat. Photonics* **15**, 456–460 (2021).
24. K. T. Kim, C. Zhang, A. D. Shiner, B. E. Schmidt, F. Légaré, D. M. Villeneuve, P. B. Corkum, Petahertz optical oscilloscope. *Nat. Photonics* **7**, 958–962 (2013).
25. A. S. Wyatt, T. Witting, A. Schiavi, D. Fabris, P. Matia-Hernando, I. A. Walmsley, J. P. Marangos, J. W. G. Tisch, Attosecond sampling of arbitrary optical waveforms. *Optica* **3**, 303–310 (2016).
26. P. Carpeggiani, M. Reduzzi, A. Comby, H. Ahmadi, S. Kühn, F. Calegari, M. Nisoli, F. Frassetto, L. Poletto, D. Hoff, J. Ullrich, C. D. Schröter, R. Moshammer, G. G. Paulus, G. Sansone, Vectorial optical field reconstruction by attosecond spatial interferometry. *Nat. Photonics* **11**, 383–389 (2017).

27. A. Leitenstorfer, S. Hunsche, J. Shah, M. C. Nuss, W. H. Knox, Detectors and sources for ultrabroadband electro-optic sampling: Experiment and theory. *Appl. Phys. Lett.* **74**, 1516–1518 (1999).
28. S. Keiber, S. Sederberg, A. Schwarz, M. Trubetskov, V. Pervak, F. Krausz, N. Karpowicz, Electro-optic sampling of near-infrared waveforms. *Nat. Photonics* **10**, 159–162 (2016).
29. E. Ridente, M. Mamaikin, N. Altwaijry, D. Zimin, M. F. Kling, V. Pervak, M. Weidman, F. Krausz, N. Karpowicz, Electro-optic characterization of synthesized infrared-visible light fields. *Nat. Commun.* **13**, 1111 (2022).
30. P. Sulzer, K. Oguchi, J. Huster, M. Kizmann, T. L. M. Guedes, A. Liehl, C. Beckh, A. S. Moskalenko, G. Burkard, D. V. Seletskiy, A. Leitenstorfer, Determination of the electric field and its Hilbert transform in femtosecond electro-optic sampling. *Phys. Rev. A* **101**, 033821 (2020).
31. N. Karpowicz, J. Dai, X. Lu, Y. Chen, M. Yamaguchi, H. Zhao, X.-C. Zhang, Coherent heterodyne time-domain spectrometry covering the entire "terahertz gap". *Appl. Phys. Lett.* **92**, 011131 (2008).
32. J. Dai, X. Xie, X.-C. Zhang, Detection of broadband terahertz waves with a laser-induced plasma in gases. *Phys. Rev. Lett.* **97**, 103903 (2006).
33. M. Porer, J.-M. Ménard, R. Huber, Shot noise reduced terahertz detection via spectrally postfiltered electro-optic sampling. *Opt. Lett.* **39**, 2435–2438 (2014).
34. M. T. Hassan, T. T. Luu, A. Moulet, O. Raskazovskaya, P. Zhokhov, M. Garg, N. Karpowicz, A. M. Zheltikov, V. Pervak, F. Krausz, E. Goulielmakis, Optical attosecond pulses and tracking the nonlinear response of bound electrons. *Nature* **530**, 66–70 (2016).
35. T. Paasch-Colberg, Ultrafast, optical-field-induced currents in solid-state materials, thesis, Technische Universität München (2014).
36. F. Lücking, A. Assion, A. Apolonski, F. Krausz, G. Steinmeyer, Long-term carrier-envelope-phase-stable few-cycle pulses by use of the feed-forward method. *Opt. Lett.* **37**, 2076–2078 (2012).
37. M. Schultze, Attosecond real time observation of ionization and electron-electron interactions, thesis, Ludwig Maximilian University of Munich (2008).
38. G. Ghosh, Dispersion-equation coefficients for the refractive index and birefringence of calcite and quartz crystals. *Opt. Commun.* **163**, 95–102 (1999).
39. T. Paasch-Colberg, A. Schiffrin, N. Karpowicz, S. Kruchinin, Ö. Sağlam, S. Keiber, O. Razskazovskaya, S. Mühlbrandt, A. Alnaser, M. Kübel, V. Apalkov, D. Gerster, J. Reichert, T. Wittmann, J. V. Barth, M. I. Stockman, R. Ernstorfer, V. S. Yakovlev, R. Kienberger, F. Krausz, Solid-state light-phase detector. *Nat. Photonics* **8**, 214–218 (2014).

**Acknowledgments:** We thank M. Weidman for helpful discussions and F. Krausz for initiating the research that created the prerequisites for this study and for helpful discussions. **Funding:** This research is based on work supported by the U.S. Air Force Office of Scientific Research under award number FA9550-16-1-0073. This work was partially supported by the Munich Centre for Advanced Photonics and by the IMPRS-APS. N.K. was partially supported by the FISR-CNR project "TECNOMED—Tecnopolo di nanotecnologia e fotonica per la medicina di precision." **Author contributions:** Conceptualization: D.A.Z. Methodology: D.A.Z. and N.K. Investigation: D.A.Z. Visualization: D.A.Z., N.K., and V.S.Y. Supervision: N.K. and V.S.Y. Writing—original draft: N.K., D.A.Z., and V. S.Y. Writing—review and editing: D.A.Z., N.K., and V.S.Y. **Competing interests:** D.A.Z. is an inventor on a patent application related to this work filed by Max Planck Innovations (no. PCT/EP2021/075105). The authors declare that they have no other competing interests. **Data and materials availability:** All data needed to evaluate the conclusions in the paper are present in the paper and/or the Supplementary Materials.

Submitted 25 July 2022
Accepted 4 November 2022
Published 21 December 2022
10.1126/sciadv.ade1029

Science Advances

# Ultra-broadband all-optical sampling of optical waveforms

Dmitry A. Zimin, Vladislav S. Yakovlev, and Nicholas Karpowicz

*Sci. Adv.*, **8** (51), eade1029.
DOI: 10.1126/sciadv.ade1029







*Science Advances* (ISSN ) is published by the American Association for the Advancement of Science. 1200 New York Avenue NW, Washington, DC 20005. The title *Science Advances* is a registered trademark of AAAS.